Electronic Supplementary Material (ESI) for Journal of Materials Chemistry A.

Supporting Information

Low electronegativity Mn bulk doping intensifies charge storage of Ni_2P redox shuttle for membrane-free water electrolysis

Zichen Liu,[ad] Gong Zhang,[b] Kai Zhang,[a] Huachun Lan,[b] Huijuan Liu[b] and Jiuhui Qu[bc]*

[a] State Key Laboratory of Environmental Aquatic Chemistry, Research Center for Eco-Environmental Sciences, Chinese Academy of Sciences, Beijing 100085, China

[b] Center for Water and Ecology, State Key Joint Laboratory of Environment Simulation and Pollution Control, School of Environment, Tsinghua University, Beijing 100084, China

[c] Key Laboratory of Drinking Water Science and Technology, Research Center for Eco-Environmental Sciences, Chinese Academy of Sciences, Beijing 100085, China

[d] University of Chinese Academy of Sciences, Beijing 100049, China

* Corresponding author e-mail: hjliu@tsinghua.edu.cn (H. Liu)

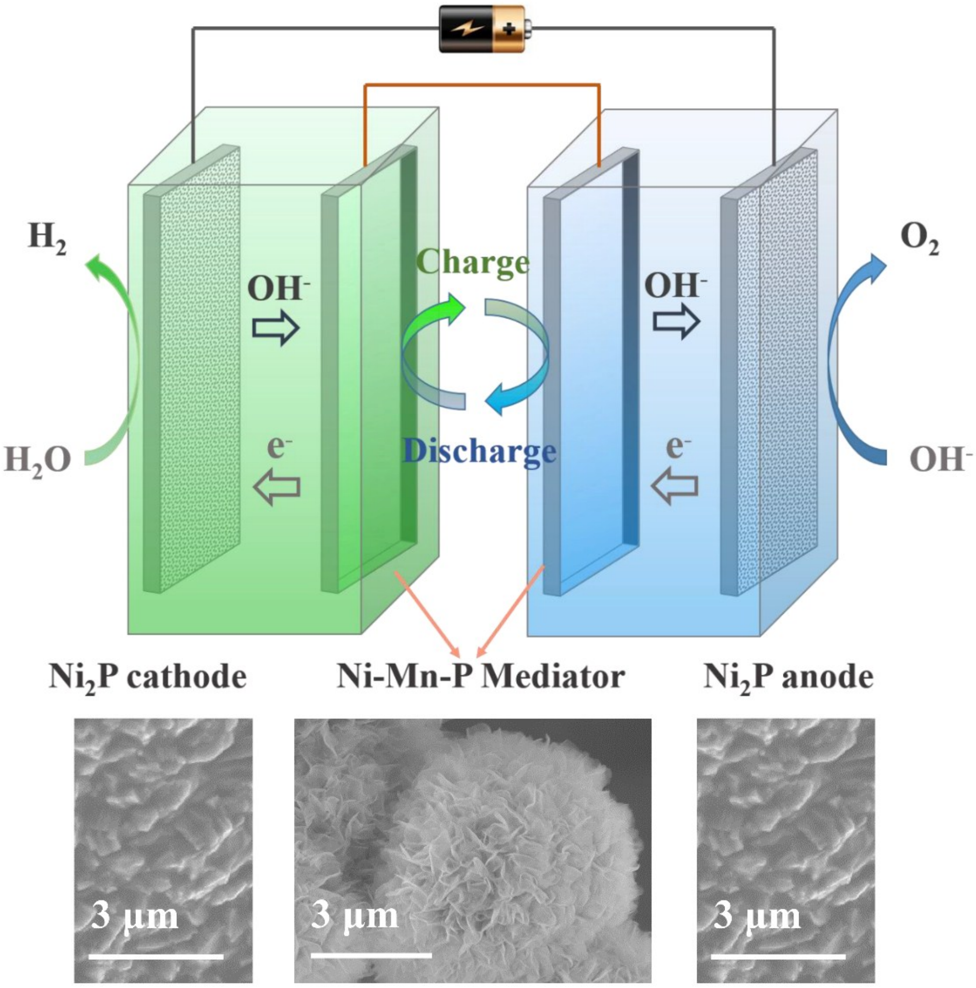

Scheme 1. Diagram of time-space-separation H_2 and O_2 with transition metal phosphides electrodes.

Supplementary Figures

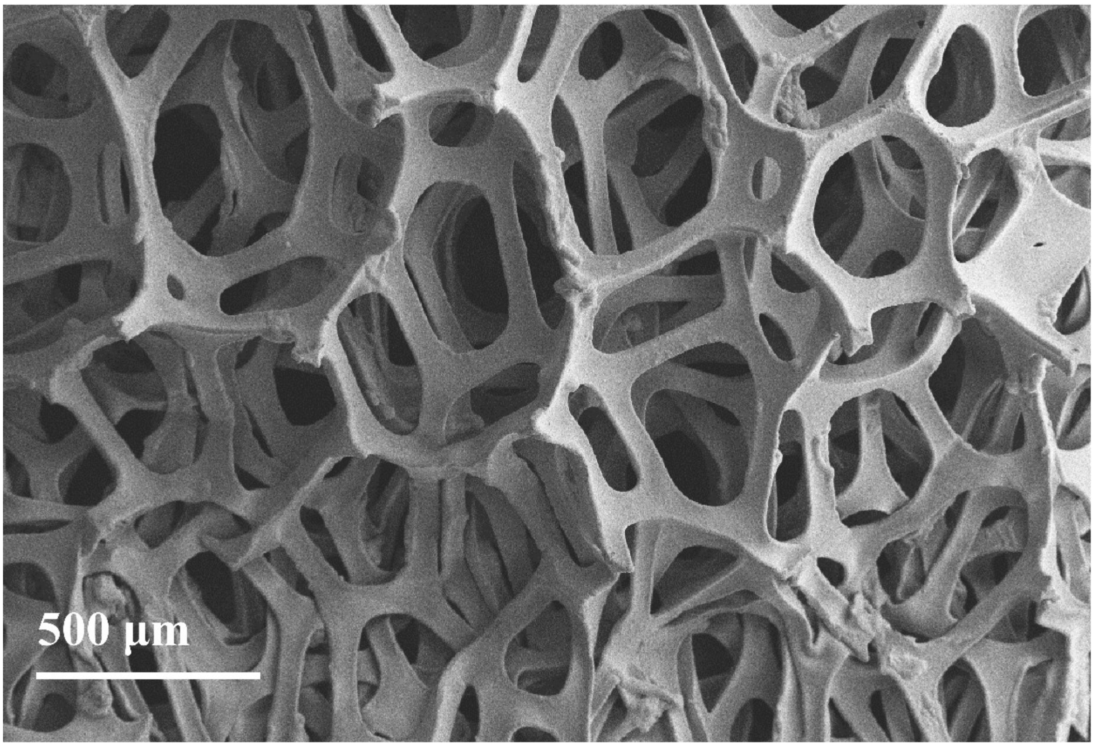

Figure S1. SEM image of the Ni foam with micropore of 200~500 µm.

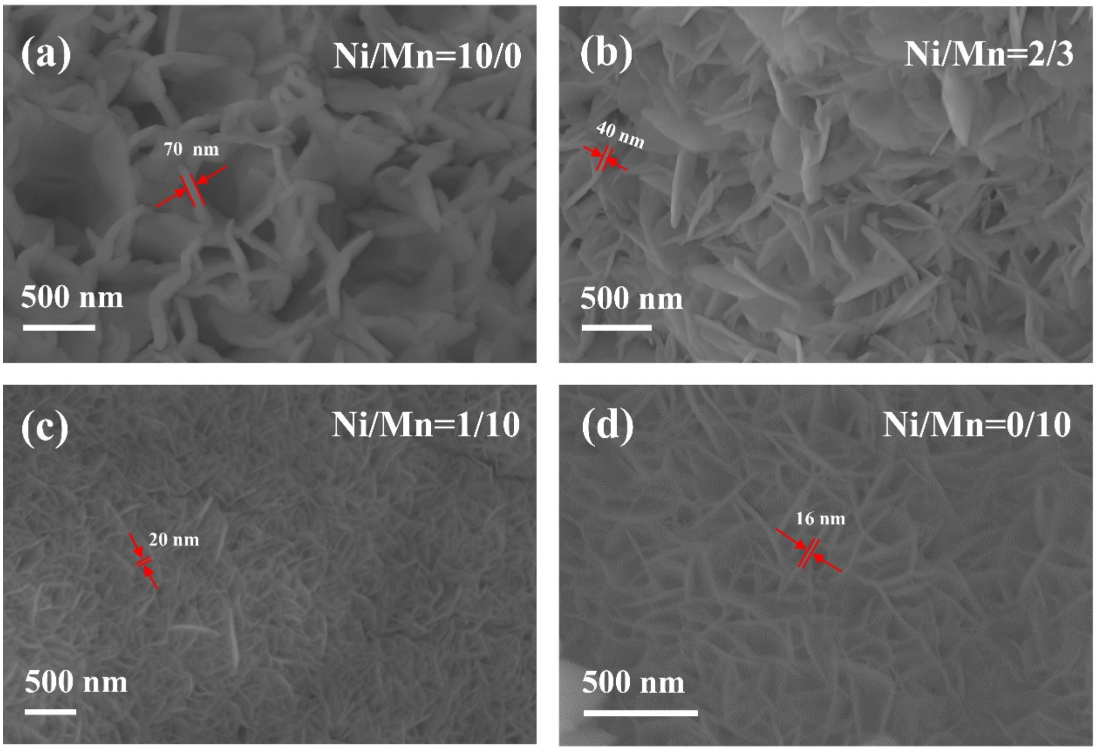

Figure S2. SEM images of hydrothermal treatment nanosheets with different Ni: Mn feeding mole ratios: (a) 10: 0, (b) 2: 3, (c) 1: 10, and (d) 0: 10. The mean thickness of different materials showed a positive correlation of the feeding mole ratios of Ni: Mn.

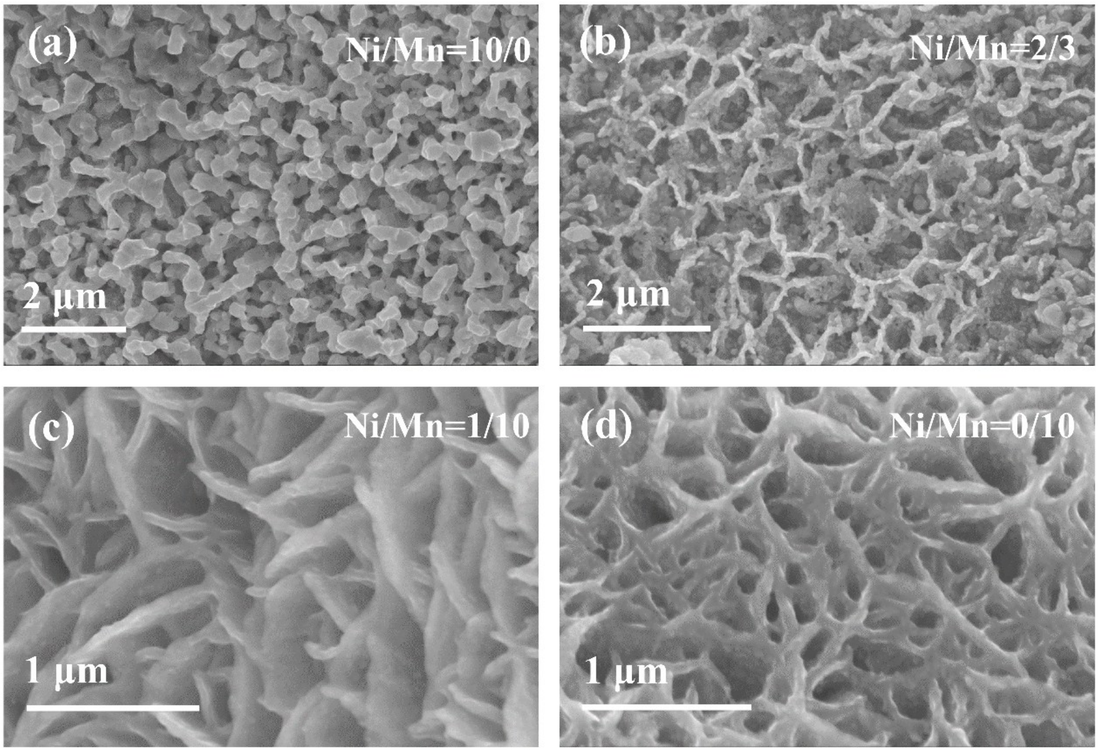

Figure S3. SEM images of Ni-Mn-P series electrodes. After phosphidation treatment, the nanosheets morphology were still retained.

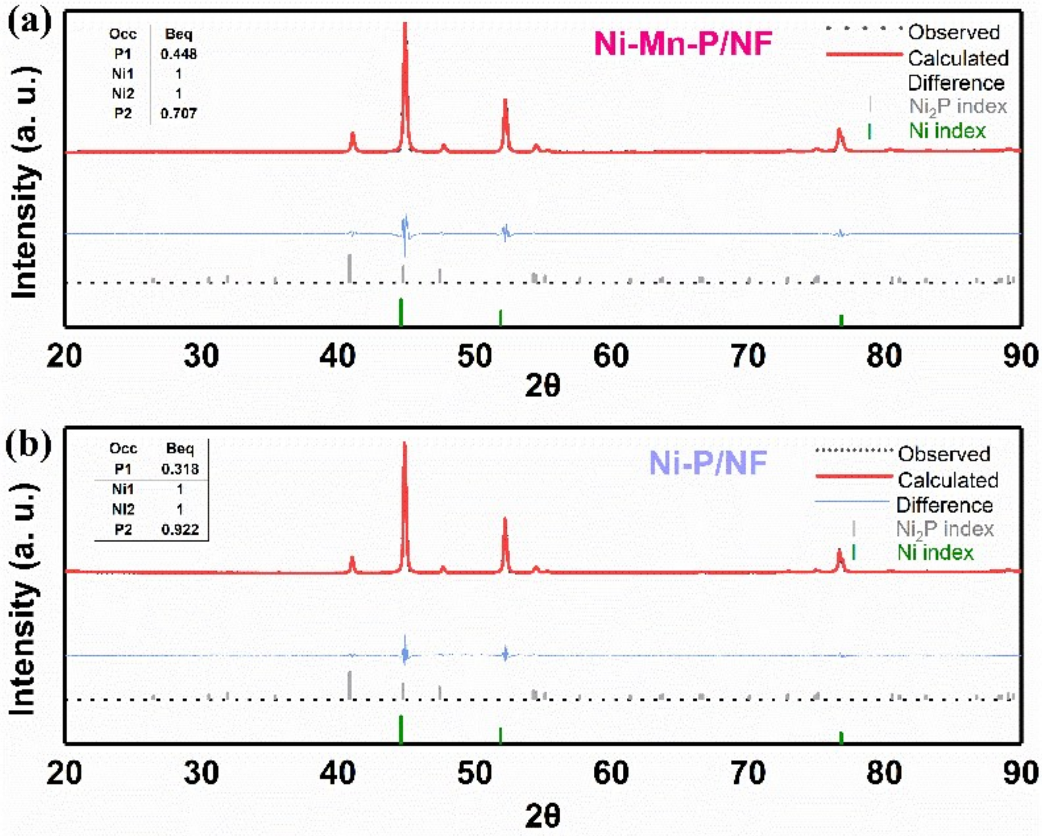

Figure S4. Rietveld-refined XRD profiles of as-prepared (a) Ni-Mn-P/NF and (b) Ni-P/NF.

The insert table reflect occupied anion sites and cation sites in Ni_2P structure.

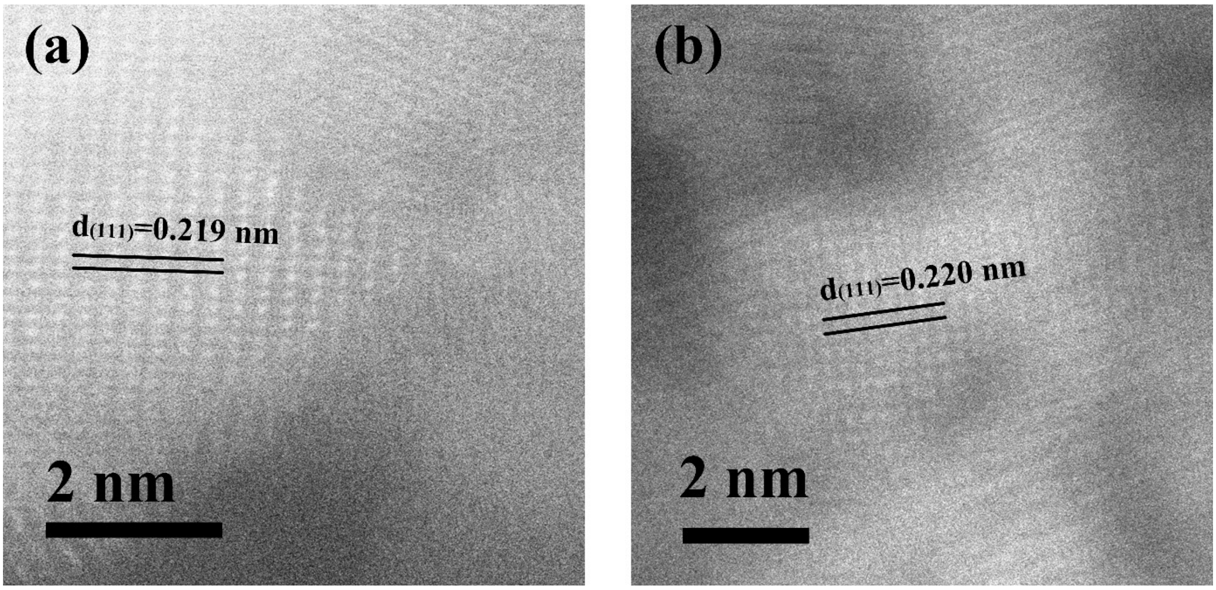

Figure S5. HAADF-STEM image of (a) Ni-Mn-P/NF and (b) Ni-P/NF

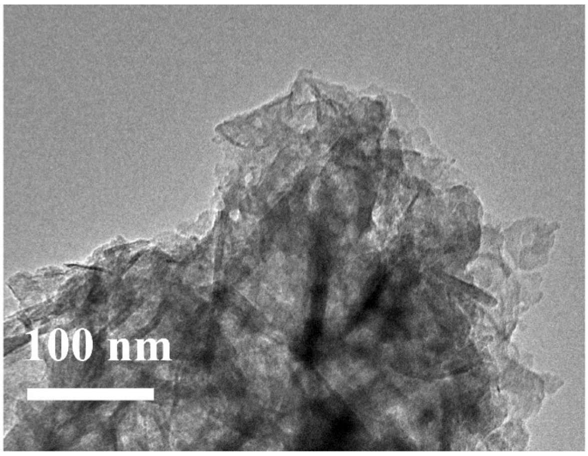

Figure S6. TEM images of 2D Ni-Mn-P nanosheets.

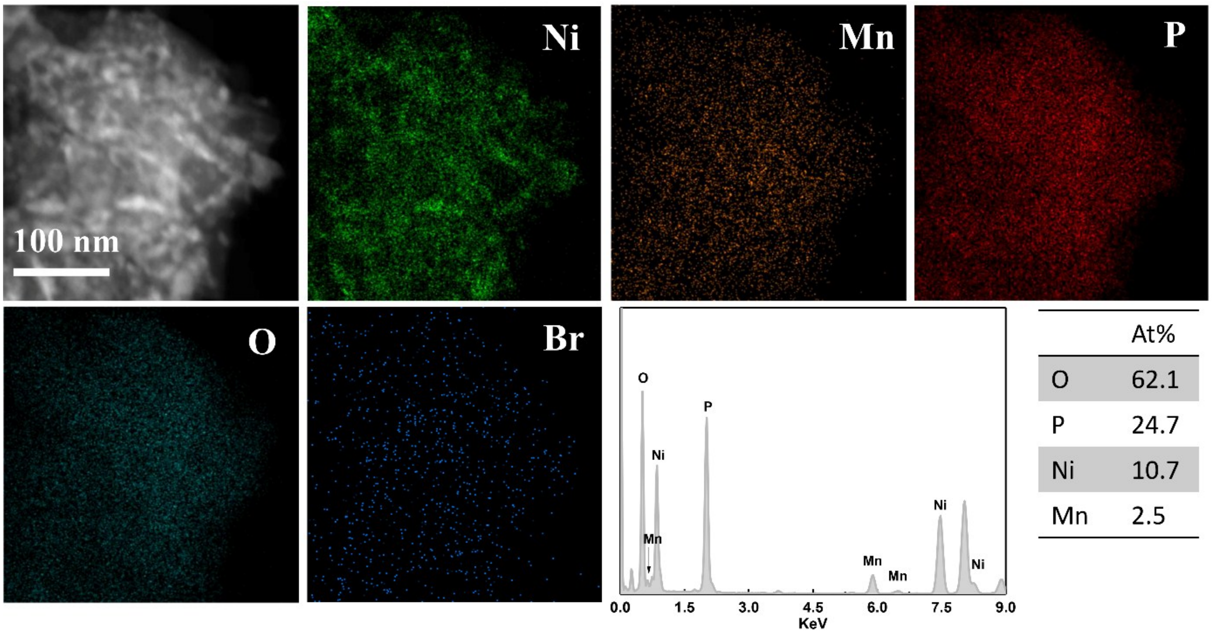

	At%
O	62.1
P	24.7
Ni	10.7
Mn	2.5

Figure S7. STEM image with corresponding EDS mapping and EDX spectrum of Ni-Mn-P/NF.

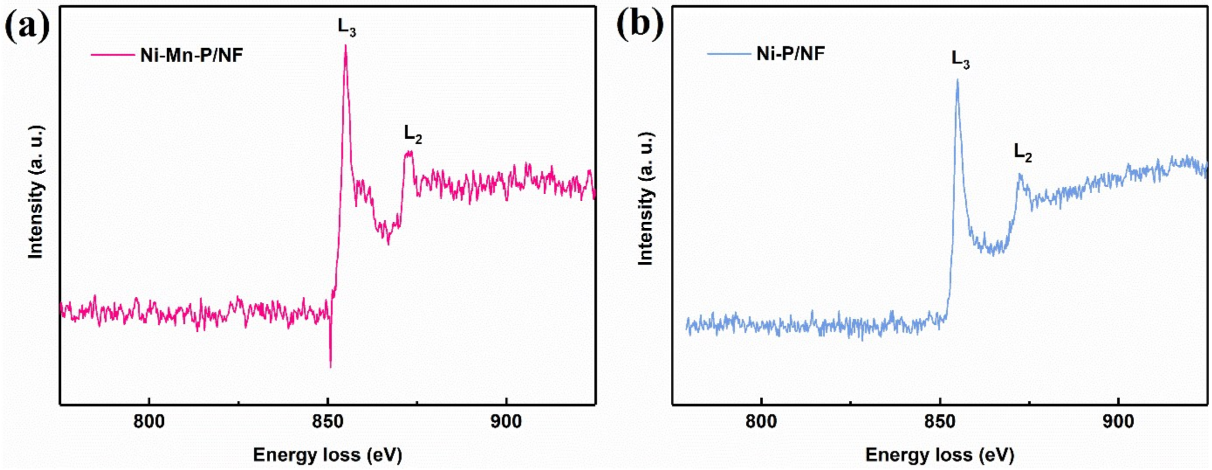

Figure S8. EELS spectra on Ni-L edges for (a) Ni-Mn-P/NF and (b) Ni-P/NF samples. Since the L_3/L_2 peak intensity ratio is inversely proportional to the transition metal valence state, the L_3/L_2 ratio of 1.65 for Ni-Mn-P and 1.62 for Ni-P demonstrate the lower valence state of Ni in Mn-doped sample.

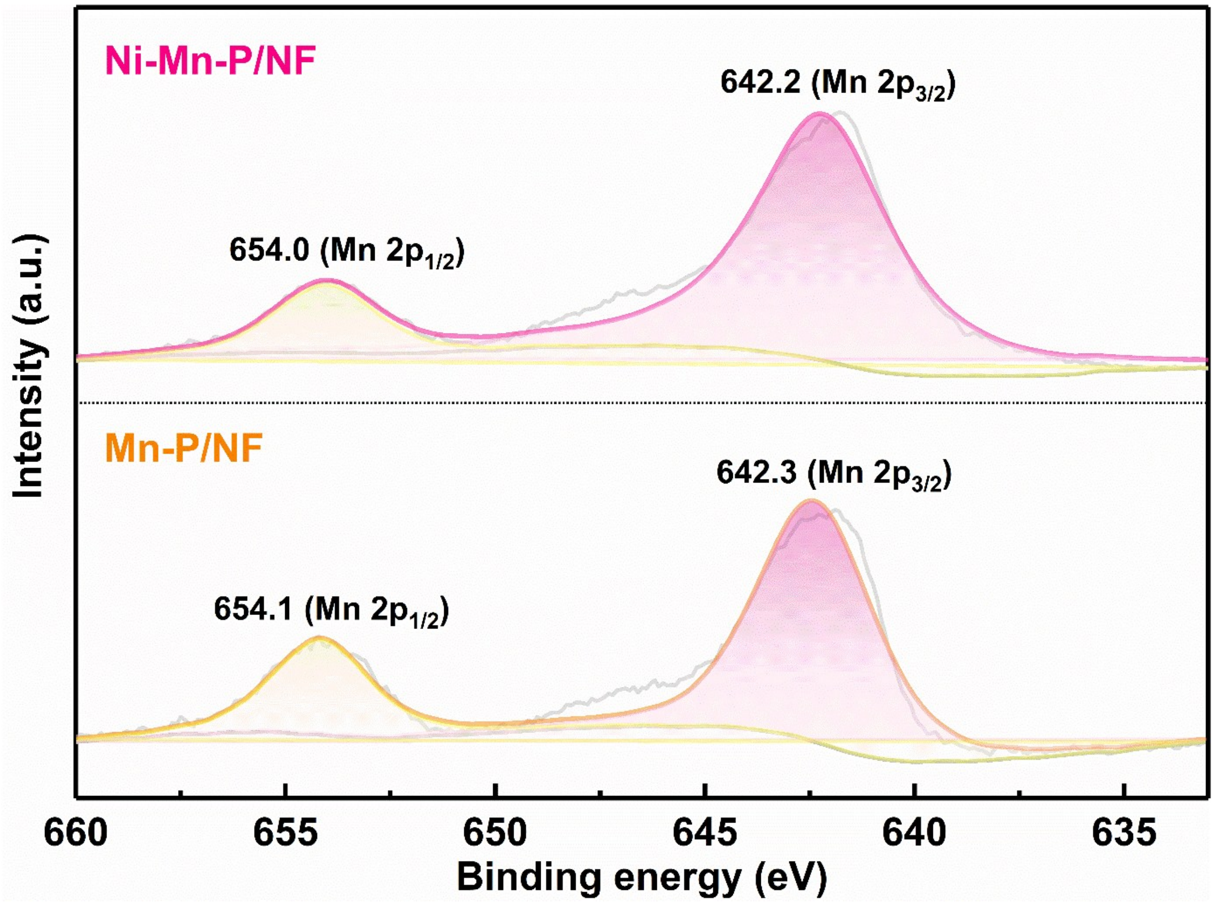

Figure S9. Mn 2p spectrum for Ni-Mn-P/NF and Mn-P/NF.

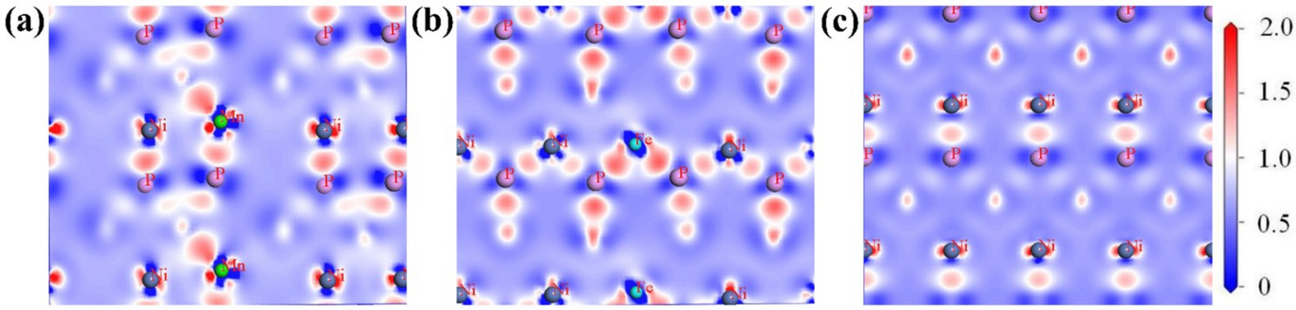

Figure S10. DFT computations on local charge density of (a) $(Ni_2Mn)_2P$, (b) $(Ni_2Fe)_2P$, and (c) Ni_2P.

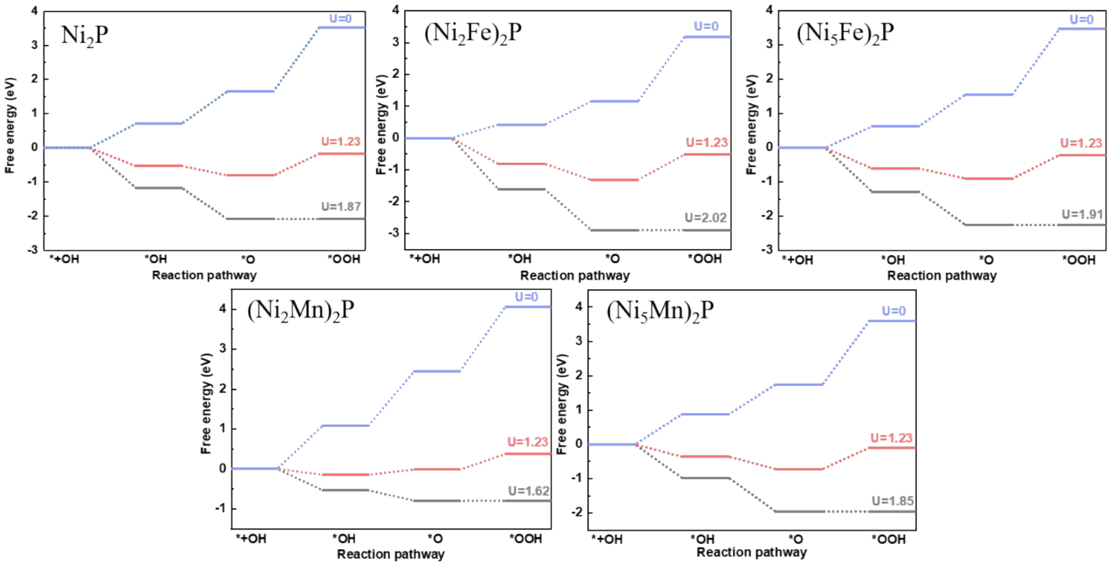

Figure S11. The free energy diagram of model structure Ni_2P, $(Ni_2Fe)_2P$, $(Ni_5Fe)_2P$, $(Ni_2Mn)_2P$, and $(Ni_5Mn)_2P$, respectively.

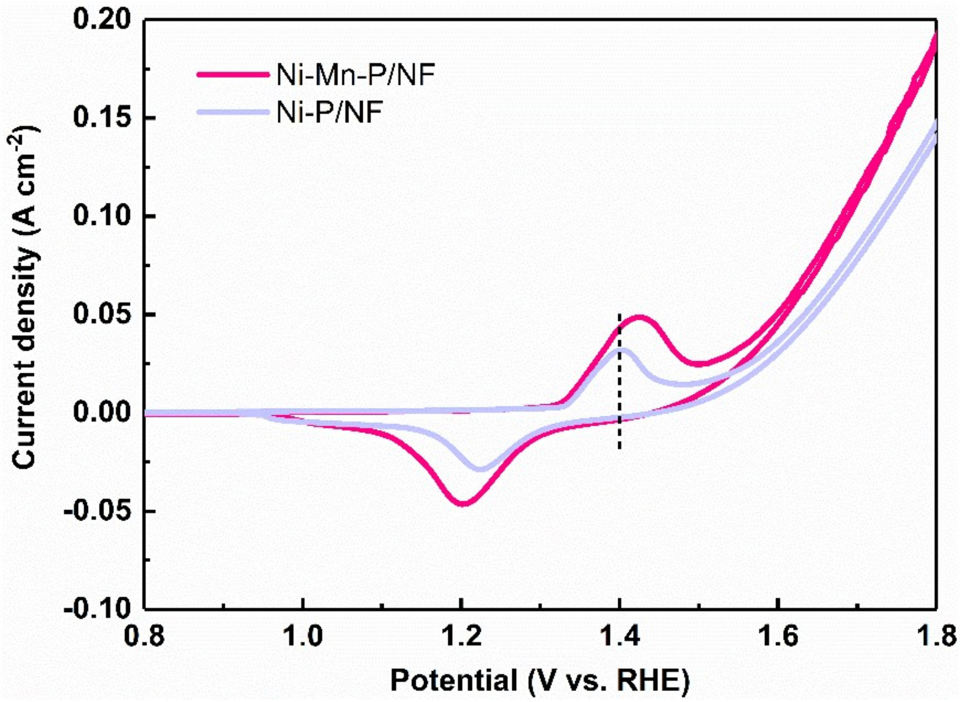

Figure S12. Cyclic voltammograms (CV) between 0.8 and 1.8 V vs RHE at the scan rate of 2mV/s .

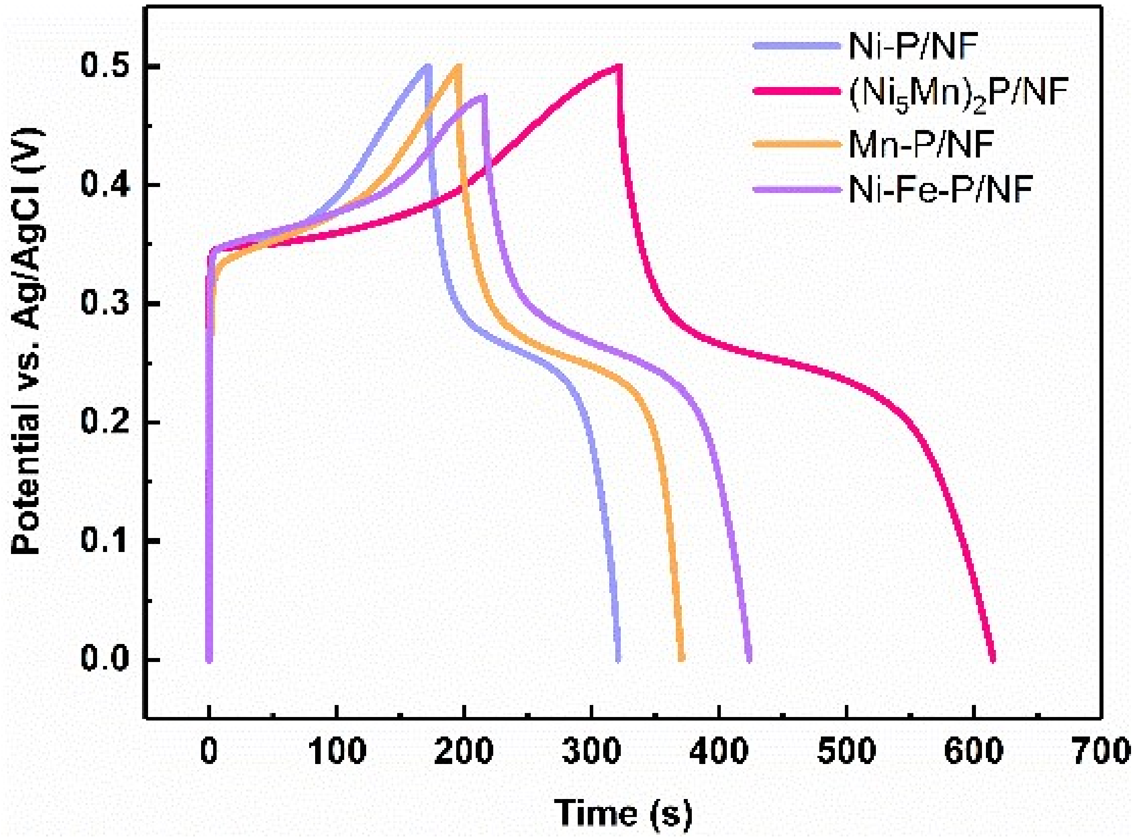

Figure S13. Galvanostatic charge/discharge curves at 3 A g^{-1} for as-prepared materials.

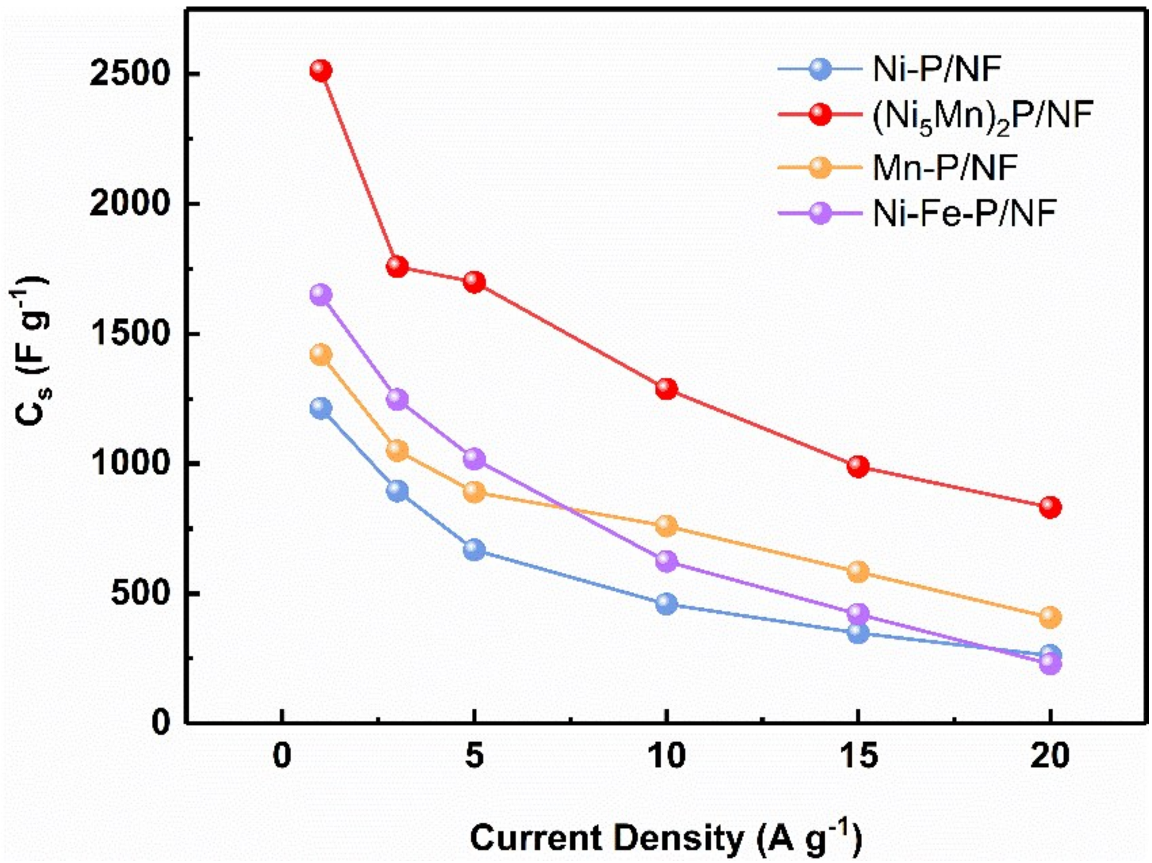

Figure S14. Comparision of C_s for Ni-Mn-P series electrodes and Ni-Fe-P electrode.

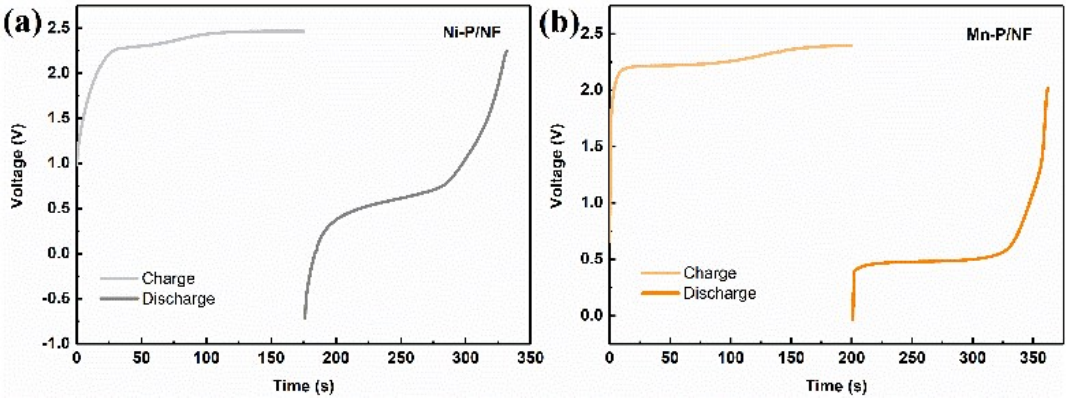

Figure S15. Two-electrode mode chronopotentiometry measurement of (a) Ni-P/NF and (b) Mn-P/NF with the applied current density of 20 mA/cm^{-2}.

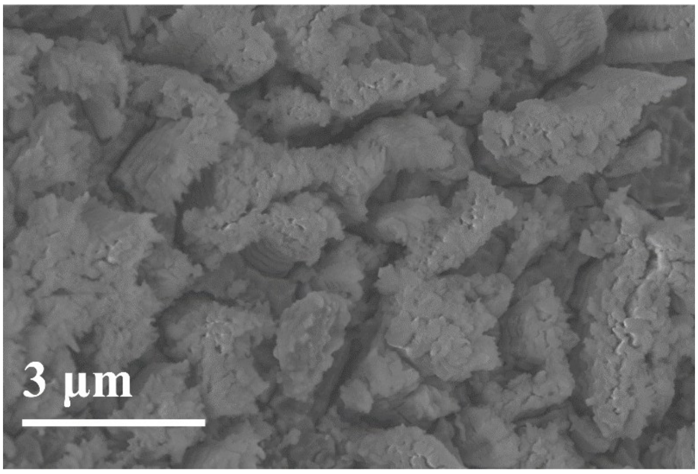

Figure S16. The SEM image for post-GCD $(Ni_5Mn)_2P$/NF in 1.0 M KOH.

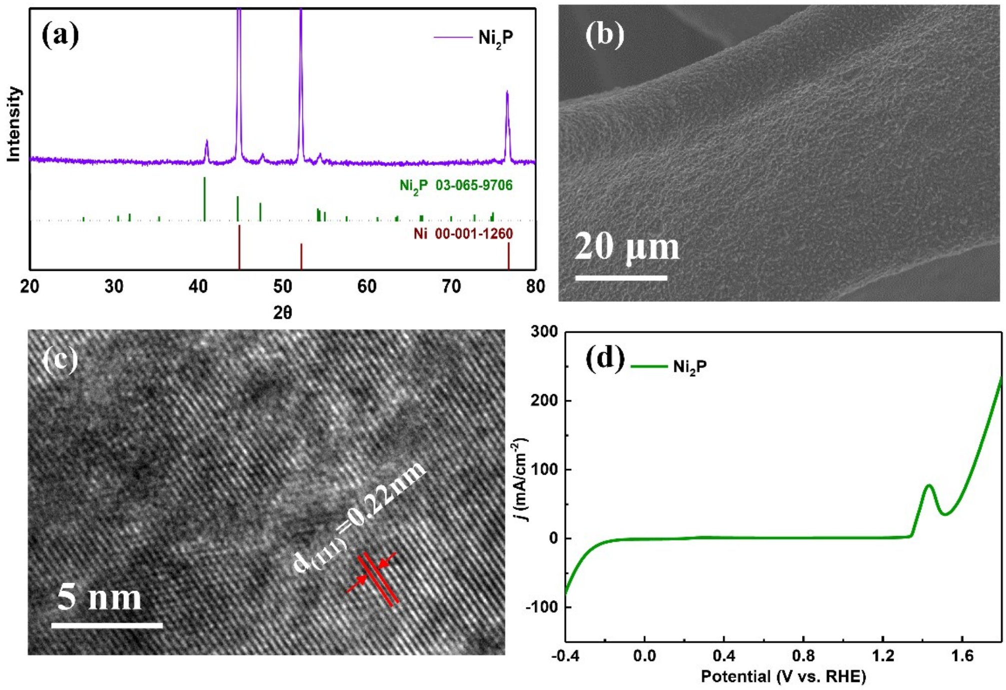

Figure S17. (a) XRD pattern of as-prepared Ni_2P/NF electrode. (b) SEM and (c) TEM images of Ni_2P/NF. (d) A consecutive LSV curve from -0.4 V to 1.8 V vs. RHE for both HER and OER measurements.

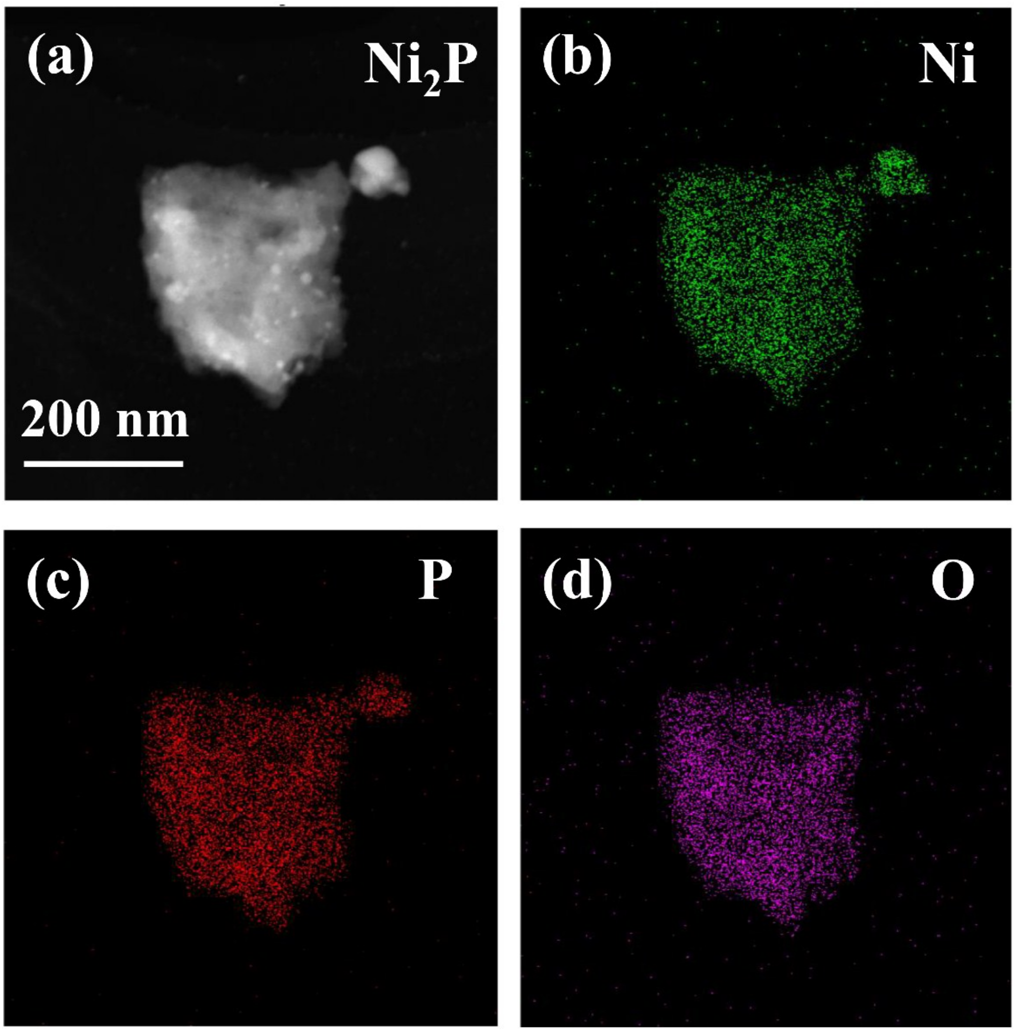

Figure S18 (a) STEM image of Ni_2P/NF with corresponding EDS mapping (b) Ni, (c) P, and (d) O.

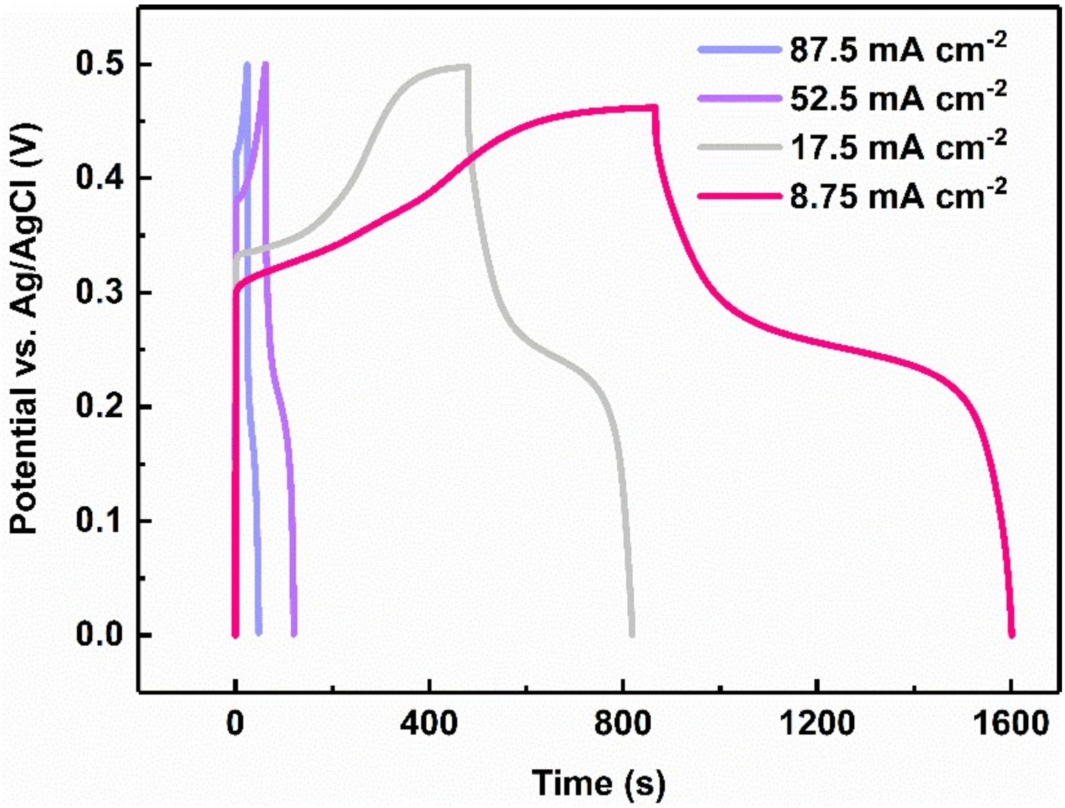

Figure S19. Galvanostatic charge/discharge curves of Ni-Mn-P mediator at different current densities.

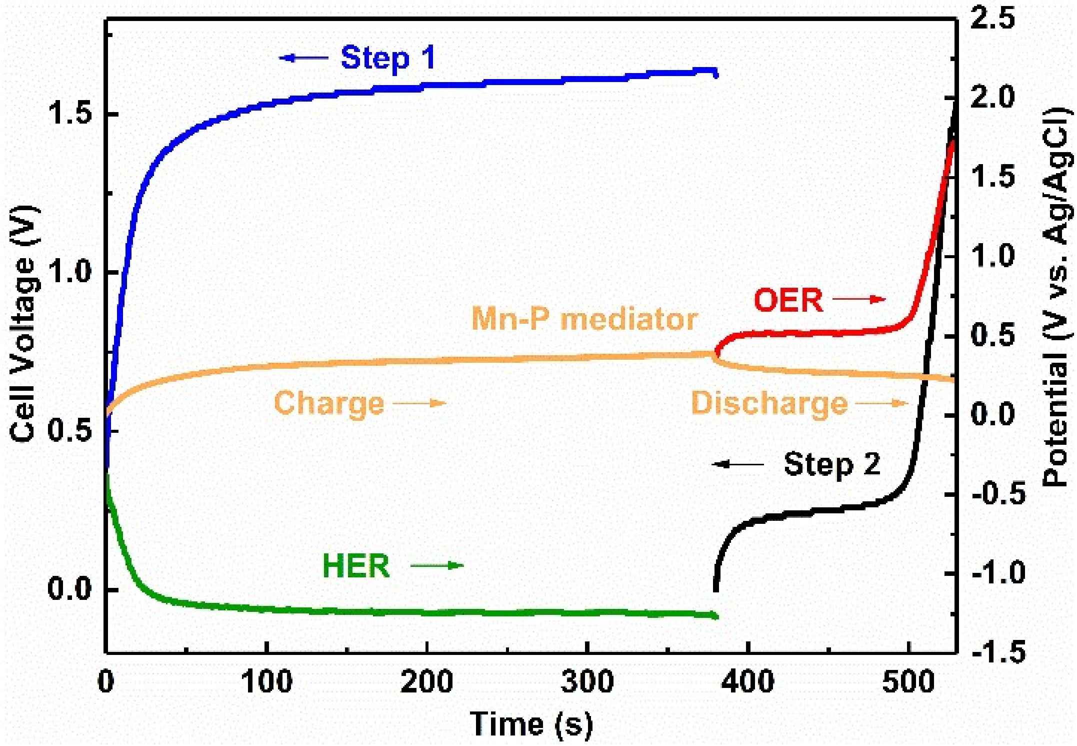

Figure S20. Chronopotentiometry curves of the electrolytic cell with Mn-P mediator at a constant applied current of 10 mA. In step 2, the cell voltage sharply increased at the end of electrolysis, due to the full discharge of the mediator.

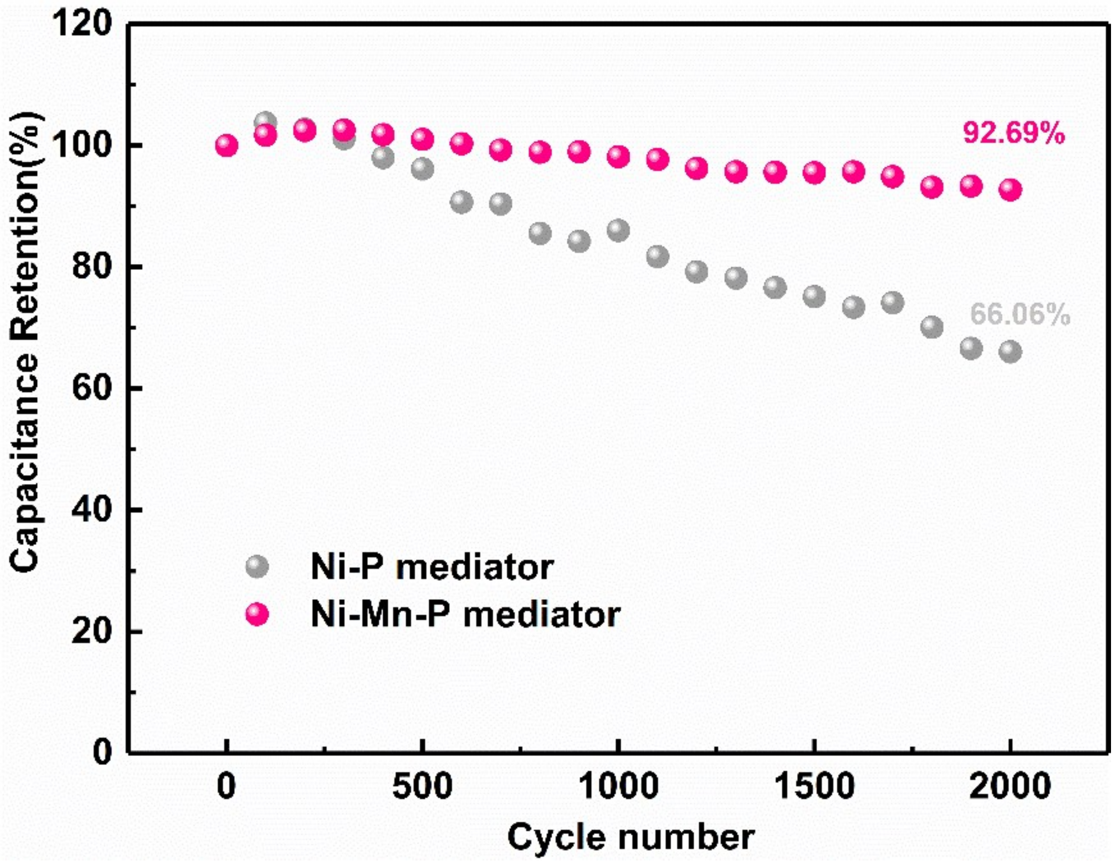

Figure S21. Cycle stability of Ni-Mn-P mediator and Ni-P mediator by the repeated GCD measurement in 2000 cycles.

Table S1. Comparison of the H_2 production time of recent solid-state mediators for decoupling water splitting.

Solid-state mediator	**HER electrode**	**OER electrode**	**Electrolyte**	**Current density (mA/mg)**	**Hydrogen production time (s)**	**References**
PTPAn	Pt-coated Ti-mesh	RuO_2/IrO_2-coated Ti-mesh	0.5 M H_2SO_4	0.15	500	Angew. Chem. Int. Ed., 2018, 57, 2904-2908
PANI	Pt-coated Ti-mesh	RuO_2/IrO_2-coated Ti-mesh	0.5 M H_2SO_4	0.025	600	J. Mater. Chem. A, 2019, 7, 13149-13153
PTO	Pt-coated Ti-mesh	RuO_2/IrO_2-coated Ti-mesh	0.5 M H_2SO_4	0.5	600	Angew. Chem. Int. Ed., 2019, 58, 4622
$Na_{0.44-x}MnO_2$	Pt-coated Ti-mesh	RuO_2/IrO_2-coated Ti-mesh[a]	1 M NaOH/ Saturated NaCl	0.05	3600	Nat. Commun., 2018, 9, 438
Ni-Mn-P	**Ni_2P**	**Ni_2P**	**1 M KOH**	**0.5**	**600**	**This work**

[a] For the chlorine evolution reaction (CER).